ELSEVIER

Carbohydrate Research 315 (1999) 222–233

CARBOHYDRATE RESEARCH

Conformational analysis of maltoside heteroanalogues using high-quality NOE data and molecular mechanics calculations. Flexibility as a function of the interglycosidic chalcogen atom

Thomas Weimar [a], Uwe C. Kreis [b], John S. Andrews [b], B. Mario Pinto [b,*]

[a] *Institut für Chemie, Medizinische Universität zu Lübeck, Ratzeburger Allee 160, 23538 Lübeck, Germany*
[b] *Department of Chemistry, Simon Fraser University, Burnaby, BC V5A 1S6, Canada*

Received 13 October 1998; accepted 5 January 1999

Abstract

The conformational analysis of three maltoside heteroanalogues containing sulfur in the nonreducing ring and either oxygen **1**, sulfur **2** or selenium **3** atoms in the interglycosidic linkage is performed using high-quality NOE data for **1**–**3** and molecular mechanics calculations using the program PIMM91 for the derivatives **1** and **2**. The compounds are substrate analogues of glucosidases and inhibit glucoamylase 2. Theoretical NOE data, obtained from Boltzmann averaging of potential energy maps from a grid search, are compared with the experimental data. The gross conformational features of all three compounds are similar in that they populate mainly two conformational regions of the potential energy maps. These two regions are equivalent to the ones found for maltose and interconvert through a rotation of the dihedral angle Ψ from $\sim -30°$ to $\sim 180°$. Experimental NOE data and theoretical energy differences and population distributions show that the substitution of oxygen with sulfur or selenium results in an increase in the flexibility of the interglycosidic linkage in the latter compounds. Thus, the population of the conformational family with a dihedral angle Ψ of $\sim 180°$ increases from $\sim 1\%$ (**1**) to $\sim 10\%$ (**2**).
© 1999 Elsevier Science Ltd. All rights reserved.

Keywords: Molecular mechanics calculations; Nuclear Overhauser enhancement; Maltose heteroanalogues; Conformational analysis; Flexibility of glycosidic linkages; Glucosidase inhibitors

1. Introduction

Carbohydrate heteroanalogues are potential inhibitors of carbohydrate-processing enzymes in that they can act as substrate analogues but yet be resistant to hydrolysis. In past years, carbohydrate analogues have been synthesised in which the ring oxygen atom is replaced by carbon, sulfur and nitrogen, and the oxygen atom in the glycosidic linkage is replaced by carbon, nitrogen, sulfur and selenium [1].

As part of a program to gain insight into the requirements for effective glucosidase inhibitors, we now present the conformational analysis of three heteroanalogues of methyl α-maltoside in which the ring oxygen atom in the nonreducing ring is replaced by sulfur and that in the glycosidic linkage is either oxygen (**1**), sulfur (**2**) or selenium (**3**) [2]. Of particular interest is the effect on flexibility of replace-

* Corresponding author. Tel.: +1-604-291-4327; fax: +1-604-291-3765.
E-mail address: bpinto@sfu.ca (B.M. Pinto)

0008-6215/99/$ - see front matter © 1999 Elsevier Science Ltd. All rights reserved.
PII: S0008-6215(99)00011-7

ment of the interglycosidic oxygen atom by heavier chalcogen atoms. High-quality NOE data on **1**–**3** and molecular mechanics calculations on **1** and **2** using the program PIMM91 [3] indicate that flexibility increases in the sequence O < S < Se.

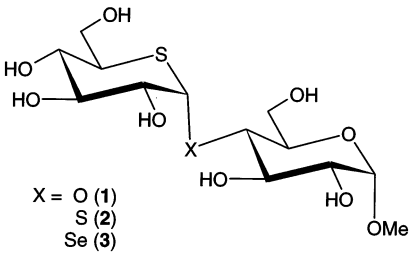

2. Results and discussion

General.—NOEs have a profound dependence on the correlation time of the molecule, with a zero crossing and a concurrent change in sign when the product of the correlation time and the spectrometer frequency is close to 1.1 [4]. Thus, molecules of the size of disaccharides, in general, show very small or no NOE enhancements at field strengths of 500 or 600 MHz in aqueous solutions. For this reason, the experimental temperature in this investigation was set to 319 K for **2** and 316 K for **1** and **3**, respectively, to decrease the viscosity of the solvent, thereby leading to faster correlation times of the molecules and permitting the measurement of accurate NOE effects. The difference in temperatures (316 and 319 K) originates from the fact that the residual water signal in the NMR spectra had to be placed relative to the anomeric proton resonances so that its influence on the integration of the NOE spectra would be negligible.

As a consequence of the substitution of oxygen in the reducing ring and/or the interglycosidic linkage with the cognate atoms sulfur and selenium, the different electronic environments of the maltoside heteroanalogues **1**–**3** result in a large dispersion of the proton resonances in these compounds (Figs. 1–3). It is interesting to note that the relative positions of the anomeric proton resonances H-1 and H-1′ for compound **1** are reversed relative to those for compounds **2** and **3**. This upfield shift in the resonance position of H-1′ in the spectra of **2** and **3** originates from the decreased electronegativities of S and Se.

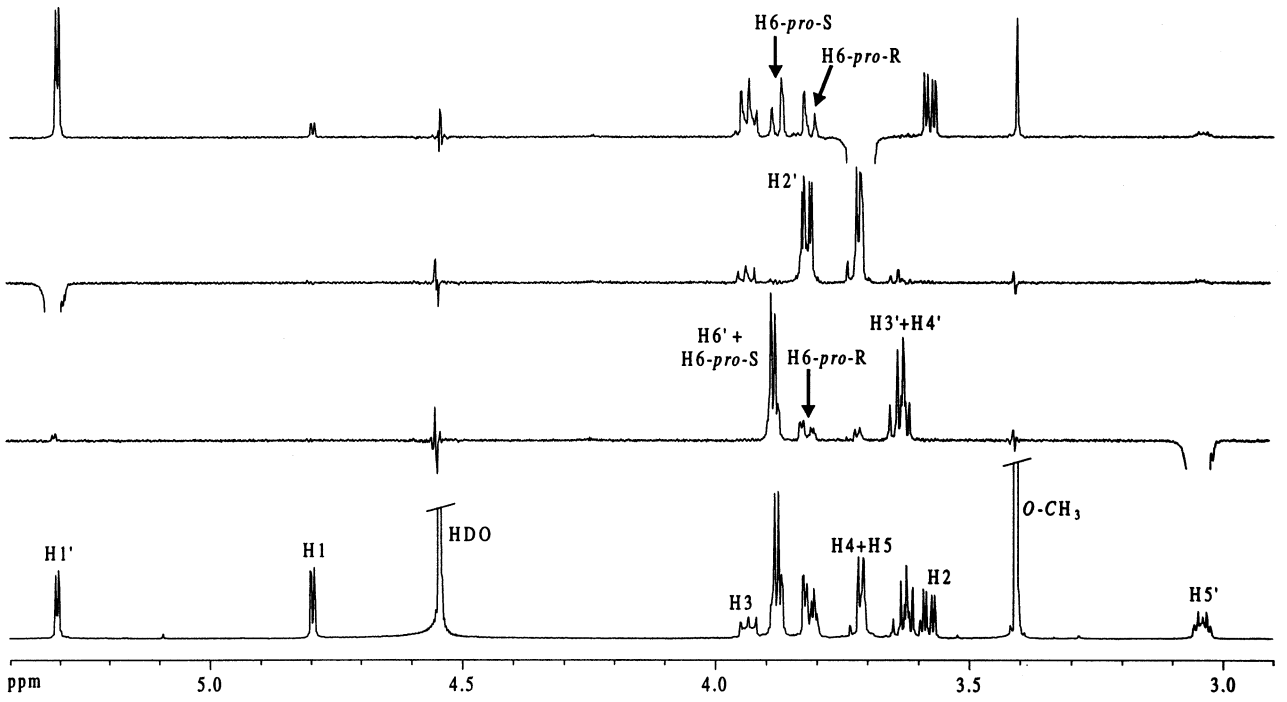

Fig. 1. 1D transient NOE spectra of compound **1**. The bottom trace shows the normal 1D spectrum. A mixing time (τ_m) of 1.34 s was used for all NOE spectra. Selective inversion was performed for the resonance signals of the protons H-5′, H-1′ and H-4 + H-5.

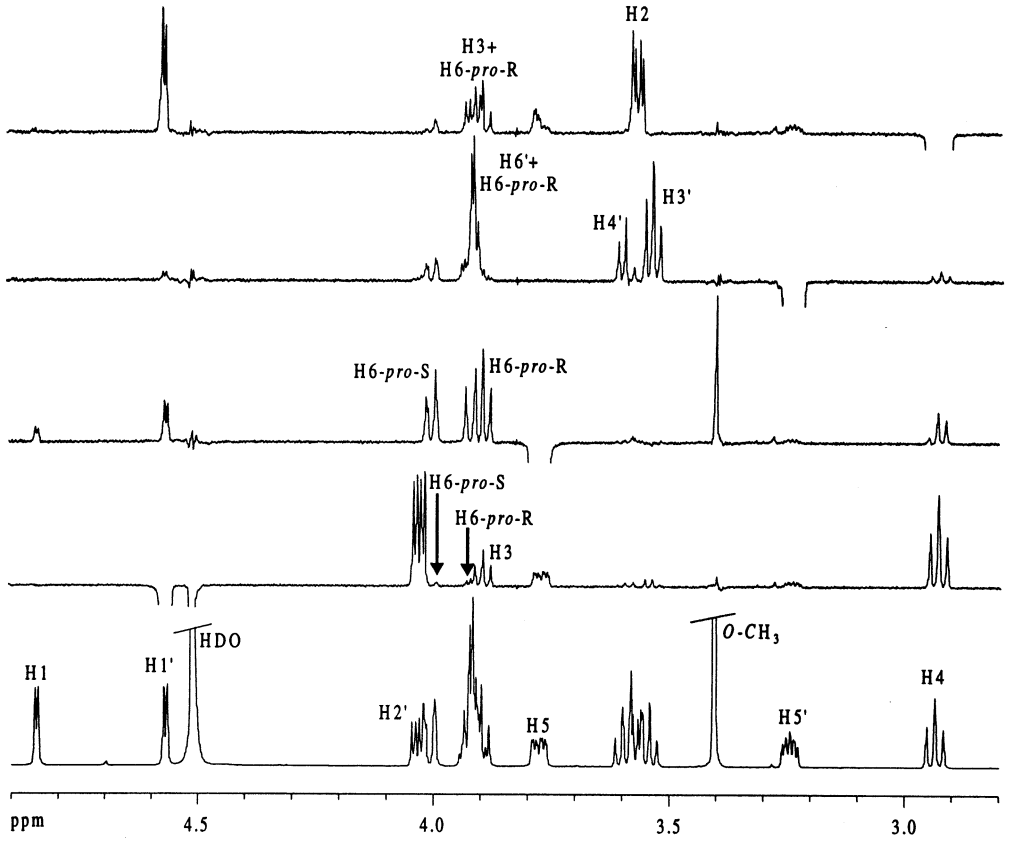

Fig. 2. 1D transient NOE spectra of compound **2**. The bottom trace shows the normal 1D spectrum. A mixing time (τ_m) of 1.34 s was used for all NOE spectra. Selective inversion was performed for the resonance signals of the protons H-1′, H-5, H-5′ and H-4.

The large dispersion observed in the spectra readily permits the investigation of the conformational behaviour of **1**–**3** in aqueous solution based on NOEs. In the parent molecule, α-maltose, most of the ring proton resonances overlap, and therefore, β-maltose was used by Shashkov et al. [5] to measure NOEs. These data, however, are limited. It has been shown for the disaccharide α-D-Fuc-(1→4)-β-D-GlcNAc-OMe, which resembles the stereoelectronic environment of maltose at the (1→4)-glycosidic linkage, that up to six NOEs across the linkage can be found [6]. These six interglycosidic NOEs (H-4{H-1′}, H-3{H-1′}, H-5{H-1′}, H-6-*pro*-R{H-5′}, H-6-*pro*-S{H-5′}, H-4{H-5′}) are also observed for the heteroanalogues investigated here (Figs. 1–3). The quality of the experimental data can be appreciated from the fact that even more very small interglycosidic effects (H-6-*pro*-R{H-1′} and H-6-*pro*-S{H-1′}) can be found for **2** (Fig. 2). The quantification of NOEs even for very small enhancements yields smooth curves, indicating a very low experimental error for the data. These experimental NOEs can be grouped into two categories, the NOEs H-4{H-1′}, H-3{H-1′}, H-5{H-1′} and H-4{H-5′} which define the population of different conformational families at the (1→4)-glycosidic linkage, and the NOEs H-6-*pro*-R{H-5′}, H-6-*pro*-S{H-5′}, H-6-*pro*-R{H-1′} and H-6-*pro*-S{H-1′} which depend on the conformation at this glycosidic linkage and the rotamer distribution at the C-5–C-6 linkage in the reducing glucose unit.

The C-5–C-6 linkages in compounds **1**–**3**.— Information about the conformational preferences at the C-5–C-6 linkages can be gained from the three-bond coupling constants ($^3J_{H,H}$) between the protons H-6-*pro*-S(R) and H-5 in the monosaccharide units. In all three compounds investigated, these coupling constants can be extracted from normal 1D or 1D transient NOE spectra for the reducing glucose unit. As indicated in Table 1, the reducing glucose units in all three disaccharides

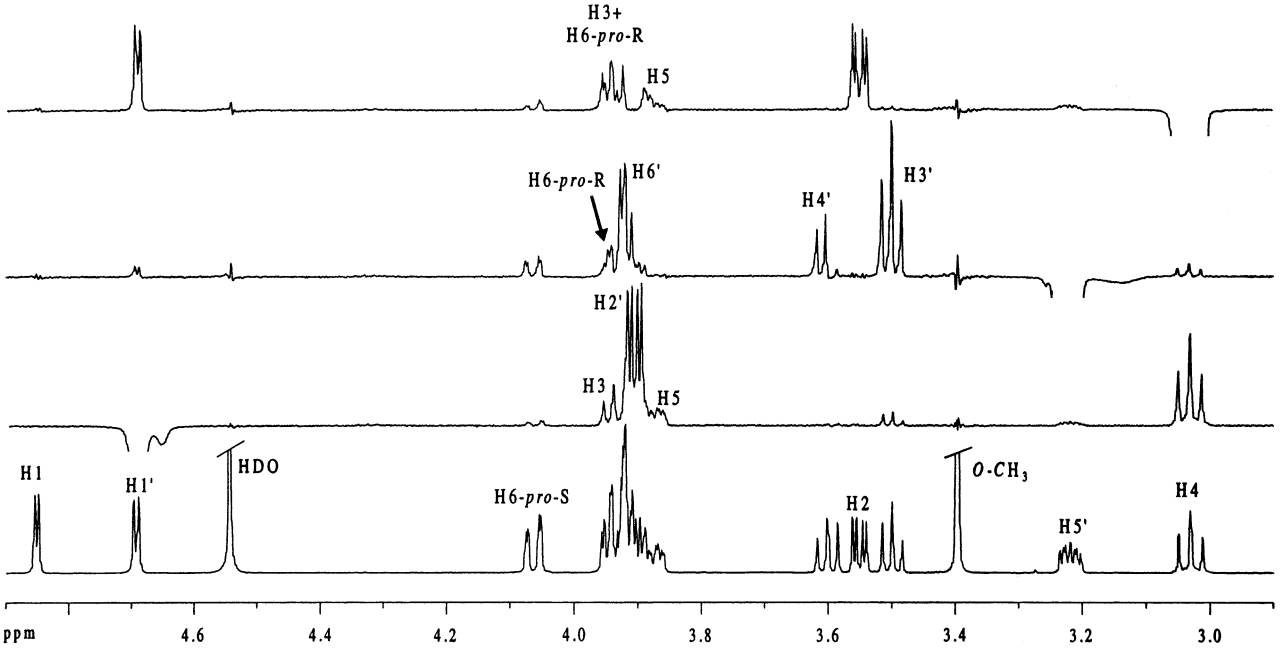

Fig. 3. 1D transient NOE spectra of compound **3**. The bottom trace shows the normal 1D spectrum. A mixing time (τ_m) of 1.34 s was used for all NOE spectra. Selective inversion was performed for the resonances of the protons H-1′, H-5′ and H-4.

show a rotameric distribution which is close to 60:40:0 for the *gg* (*gauche*/*gauche*), *gt* (*gauche*/*trans*) and *tg* (*trans*/*gauche*) orientations at these hydroxymethyl groups. Slight differences can be found between **1**, which has a normal reducing glucose unit, compared with **2** and **3** in which oxygen in the glycosidic linkage is replaced by sulfur or selenium, respectively. In **2** and **3**, the coupling constants imply a higher ratio of *gt*-conformations that might stem from the stereoelectronic modification at the glycosidic linkage which is in close proximity to these C-5–C-6 bonds. Unfortunately, it is not possible to differentiate the resonances of the prochiral protons H-6-*pro*-R(S) of the hydroxymethyl group in the 5-thioglucose units since the chemical shift of these protons is degenerate and, therefore, no information on the conformational preferences about these C-5–C-6 bonds can be gained from the coupling constants.

In contrast to this experimental finding, a Boltzmann averaging of all calculated conformations from a grid search showed a high

Table 1
Experimental $^3J_{\text{H-5/H-6-}pro\text{-R(S)}}$ coupling constants and calculated rotamer distributions at the C-5–C-6 linkage in the reducing glucose unit of **1**–**3**[a]

Compound and proton	$^3J_{\text{H-5/H-6-}pro\text{-R(S)}}$ (Hz)	Calculated rotameric distribution *gg*:*gt*:*tg* (%)		
		Method A[b]	Method B[c]	Method C[d]
1 H-6-*pro*-R	4.8			
1 H-6-*pro*-S	1.8	66:34:0	78:27:−5	69:46:−15
2 H-6-*pro*-R	5.4			
2 H-6-*pro*-S	2.1	58:40:2	67:35:−2	59:52:−11
3 H-6-*pro*-R	5.4			
3 H-6-*pro*-S	2.2	58:39:3	67:34:−1	60:50:−10

[a] Experimental values have been extracted from normal 1D and 1D transient NOE spectra.
[b] Gerlt and Youngblood [7].
[c] Streefkerk et al. [8].
[d] Haasnoot et al. [9].

population of the *tg*-conformation (55:10:35 for **1** and 33:17:50 for **2** (*gg*:*gt*:*tg*)) at the reducing C-5–C-6 bond in compounds **1** and **2**. This preference for the *tg*-orientation at the C-5–C-6 linkage in molecular mechanics calculations of glucose units is a problem that is encountered frequently [10]. It often stems from the neglect of the influence of solvent molecules (water) in these calculations [10a, 11] or from an incomplete parameterisation of the force field for the O–C–C–X linkage [12]. Since *tg*-conformations seem to be populated only to ca. 1–3% (Table 1), it is clear that this overestimation of *tg*-conformations has a dramatic impact on all theoretical NOE data involving the prochiral protons of the hydroxymethyl groups. To overcome this problem, Boltzmann averaging was performed again, neglecting all *tg*-conformers [13] and using ~10,000 conformations from the grid search. The rotameric distributions at the C-5–C-6 linkages now changed to ratios of 85:15 (*gg*:*gt*) for **1** and 70:30 (*gg*:*gt*) for **2**, which much better represent the experimental findings. As a consequence of this modification, the relative population distributions of the different regions of conformational space changed to give slightly higher populations for the global minimum energy region **A** (see Fig. 4), which resulted in an improved fit between experimental and theoretical NOE data (data not shown). It is noteworthy that the solid-state structure of **2** derived by X-ray crystallography [14] shows a *gg* and *gt* preference for the C-5–C-6 linkage in the reducing and nonreducing units, respectively (see Fig. 5 and Table 2).

The following discussion and comparison of experimental and theoretical NOE data make use of the Boltzmann-averaged data, neglecting the *tg*-conformations. However, the neglect of all *tg*-conformations is a severe modification of the original grid search data and it is clear that even small changes in the rotameric distribution will have a marked effect for all theoretical NOEs involving the prochiral protons at the C-5–C-6 linkages. Therefore, the differences between theoretical and experimental NOEs involving the H-6-*pro*-R(S) protons at the reducing glucose unit will not be discussed here in great detail.

Modelling of the glycosidic linkage. Compound **1**.—We have previously reported that PIMM91 accurately depicts the glycosidic linkage distribution in a 5′-thio analogue of kojibiose and have found very good agreement between the experimental NOE data and theoretical data from Boltzmann averaging of con-

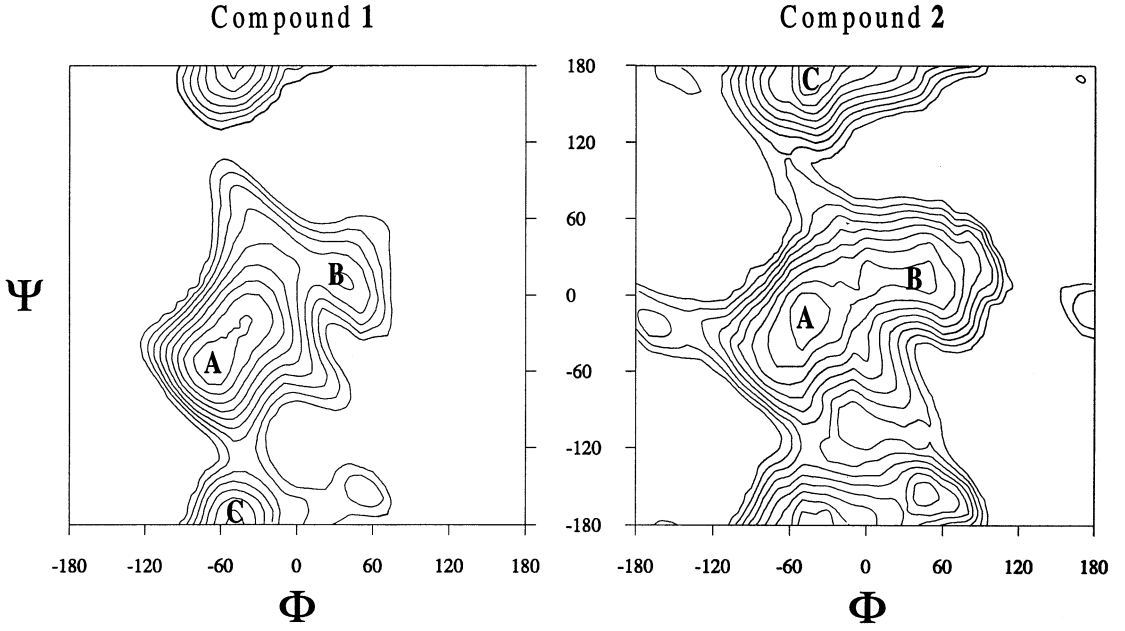

Fig. 4. Potential energy maps for compounds **1** and **2** with a spacing of 1 and a cutoff of 10 kcal mol^{-1}. Minimum-energy conformations (kcal mol^{-1}) for the regions **A**–**C** are found at Φ/Ψ angles of $-69°/-58°$ (0.0), 20°/35° (6.9) and $-51°/178°$ (3.5) for compound **1** and $-49°/-18°$ (0.0), 13°/27° (2.2) and $-50°/180°$ (1.6) for compound **2**, respectively.

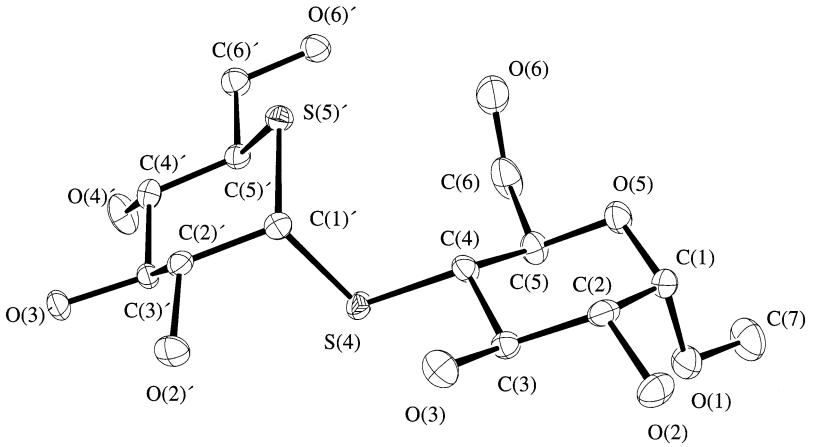

Fig. 5. Molecular structure of **2** derived by X-ray crystallography [14].

formations obtained in a grid search [1h]. In compound **1** a similar situation at the α-(1→4)-glycosidic linkage occurs in that the ring oxygen in the nonreducing unit is replaced by sulfur; we therefore expected to find good agreement between experimental and theoretical Boltzmann-averaged grid search NOE data.

Fig. 6 shows the comparison of selected experimental NOE curves with theoretical curves calculated from the Boltzmann-averaged grid search and from two minimum energy conformations that represent the conformational families **A** and **C** in the potential energy map (Figs. 4 and 7). An overall correlation time of 80 ps was used in the full relaxation matrix calculations for all theoretical curves. This correlation time yielded a very good fit for the intraglycosidic NOEs in the two ring systems. Fig. 6 indicates that the shapes and values of the theoretical intraglycosidic NOE curves are almost independent of the model used (averaged grid search or single conformational family). This is not the case for the interglycosidic NOE curves where the different conformations or conformational distributions give rise to a large variation in the theoretical data.

Comparison of the experimental interglycosidic NOE curves with the theoretical ones does not show the same agreement observed for the intraglycosidic NOE effects; in fact, the theoretical data have quite large discrepancies from the experimental ones. These discrepancies can be understood by analysing the potential energy map of this molecule, which is displayed in Fig. 4. Boltzmann averaging of all *gg*- and *gt*-conformational states predicts a probability of 98% for conformations in region **A**, only ~0.5% for conformations in region **B** and ~1% for conformations in region **C**. Also, the minimum-energy conformation is found at Φ/Ψ angles of $-69°/-58°$. About this conformation, the proton pairs H-1′–H-3 and H-5′–H-4 come into close proximity (~2.8 Å for H-1′–H-3 and H-5′–H-4), thus increasing the averaged values of these theoretical NOEs. It is the over-representation of calculated low-energy conformations in the region of Φ/Ψ values around $\sim -60°/-60°$

Table 2
Selected structural data for methyl 4,5′-dithio-α-maltoside **2** [14]

Φ (°)	H-1′–C-1′–S-4–C-4	−36
	C-2′–C-1′–S-4–C-4	−154.9(2)[a]
	S-5′–C-1′–S-4–C-4	+80.7(1)
Ψ (°)	C-1′–S-4–C-4–H-4	−6
	C-1′–S-4–C-4–C-3	+111.5(2)
	C-1′–S-4–C-4–C-5	−125.8(2)
ω_1 (°)	S-5′–C-5′–C6′–O-6′	+59.5(2)
ω_2 (°)	O-5–C-5–C-6–O-6	−59.8(2)
Bond angles (°)	C-6′–C-5′–S-5′	107.58(21)
	C-5′–S-5′–C-1′	99.15(13)
	S-5′–C-1′–S-4	113.72(15)
	C-1′–S-4–C-4	100.44(14)
Bond lengths (Å)	C-5′–S-5′	1.818(3)
	S-5′–C-1′	1.8199(25)
	C-1′–S-4	1.821(3)
	S-4–C-4	1.826(3)

[a] The numbers in parentheses indicate the standard deviation in the last digits.

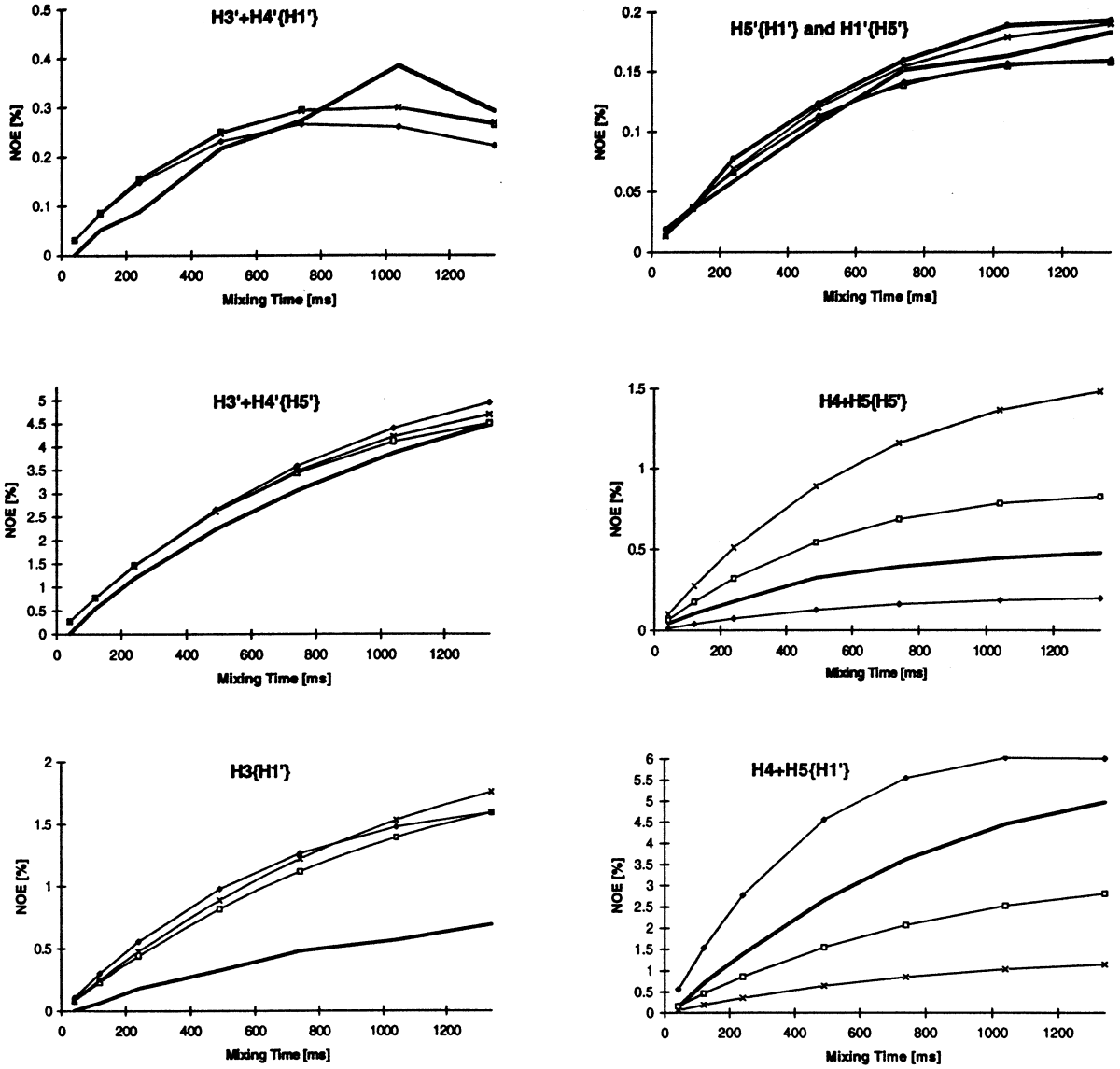

Fig. 6. Comparison of selected experimental and theoretical NOE curves for compound **1**. Experimental values are plotted with thick lines. Theoretical NOE curves represent (1) a Boltzmann averaging of grid search data neglecting all *tg*-conformations (—□—), (2) the global minimum-energy conformation **A** (Φ/Ψ $-69°/-58°$) (— × —), and (3) the local minimum-energy conformation **C** (Φ/Ψ $-51°/178°$) (—◆—).

(minimum **A**) that is responsible for the discrepancy between the Boltzmann-averaged and the experimental NOE data. The same arguments can be used to explain the similarity of all theoretical NOE curves for the NOE H-3{H-1′}. In the conformation that was used to calculate the NOE curve for the local energy minimum **C** (Φ/Ψ $-51°/178°$), the protons H-1′ and H-3 also show a distance of ~ 2.9 Å and, as a consequence, all three theoretical NOE curves are similar.

Compound **2**.—The situation is different for compound **2** in which not only the intraglycosidic NOEs show good agreement between experimental and theoretical values but also the interglycosidic NOE H-4{H-1′} is accurately represented by the Boltzmann-averaged grid search curves (Fig. 8). However, the calculated NOE curve based on the global minimum-energy conformation **A** (Φ/Ψ $-49°/-18°$) shows an even better fit to the experimental curve. If other interglycosidic NOEs had not been observable, this finding could have led to the erroneous conclusion that compound **2** is

represented entirely by this global minimum-energy conformation. Since many more interglycosidic NOEs are found for **2**, it is readily obvious that the conformational features of this compound have to be interpreted as an average over different conformational states. For **2**, the Boltzmann averaging of the *gg*- and *gt*-conformations predicts populations of 70%, 18% and 9% for regions **A** to **C**, respectively, thus indicating much more flexibility compared with the conformational model of **1**. Secondly, conformations with glycosidic torsion angles Φ/Ψ of $\sim -60°/-60°$ already have a potential energy of ca. 2 kcal mol^{-1} (compare with Fig. 4), which reduces the contribution of conformations in this region to the theoretical NOEs H-3{H-1′} and H-4{H-5′}. However, a detailed comparison of experimental with theoretical data suggests that the calculated model is still slightly too restricted to accurately represent the experimental data. Thus, the NOEs H-5{H-1′} and H-4{H-5′} seem to be under-represented in the theoretical Boltzmann-averaged data, which points to an under-representation of conformations in the region of $\Phi/\Psi \sim -60°/-60°$ and region **C**. A higher population of these two conformational families would enhance the NOEs H-5{H-1′} and H-4{H-5′}, thus improving the fit between experimental and theoretical Boltzmann-averaged data. The NOE H-3{H-1′} can only be used as a rough indicator of the population distributions, since the experimental data have been extracted by line deconvolutions of the original NOE spectra. However, the agreement between the experimental and different theoretical data for this NOE is good.

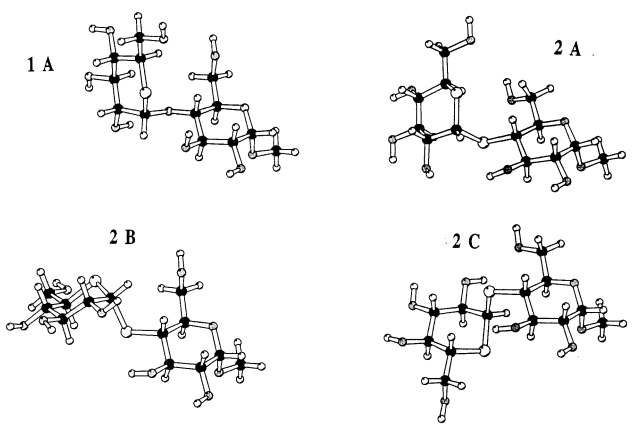

Fig. 7. Ball-and-stick representations of conformations of compounds **1** and **2**, namely minimum **A** of compound **1** and minima **A**–**C** of compound **2**. Plots have been produced with the program MOLSCRIPT [15].

The global minimum-energy structure of compound **2**, region **A** ($\Phi/\Psi \sim -50°/-20°$), coincides with the structure derived by X-ray crystallography (Fig. 5 and Table 2) [14]. The solid-state conformation indicates further, that in accord with expectations based on the anomeric effect, the S-5–C-1–S-1 bond angle is greater than tetrahedral [16] and the torsional preference about the Φ angle is consistent with expectations based on the exo-anomeric effect [17].

Experimental evidence for increased flexibility in the sequence **1** < **2** < **3**.—In all three compounds investigated here, the intraglycosidic NOEs H-3′ + H-4′{H-5′} can be used to normalise the interglycosidic NOEs H-4{H-1′}, H-3{H-1′} and H-5{H-1′} so that a direct comparison of the relative flexibility of these glycosidic linkages may be achieved. Fig. 9 indicates that, although the interglycosidic bond length increases from **1** to **3**, the relative NOEs H-3{H-1′} and H-5{H-1′} in compounds **2** and **3** are larger than in **1**. Concurrently, the relative NOE H-4{H-1′} decreases from **1** to **3**. This finding is in agreement with the molecular mechanics calculations, which show a decrease in the potential energy differences between the minimum energy regions **A** and **C** (compare with Fig. 4) in **2** as compared with **1**. Taking the Boltzmann-averaged data for **1** and **2** as an estimate of conformations in the region of Ψ-angles around 180°, these conformations are populated to the extent of $\sim 1\%$ and $\sim 10\%$ in compounds **1** and **2**, respectively. Bock et al. [18] have also noted an increase in the population of the inverted conformation **C** in 4-thiomaltosides relative to the parent maltosides.

As a final point of interest, we comment on the increased tolerance for alternative conformations about the acetal centres in the heavier congeners **2** and **3**. The conformational preferences about the acetal centre are dictated by the anomeric effect, which refers to the torsional preferences about the C–X and C–Y bonds in $RX–CH_2–YR'$ molecules. In axially oriented compounds, the *gauche*, *gauche* **4** is

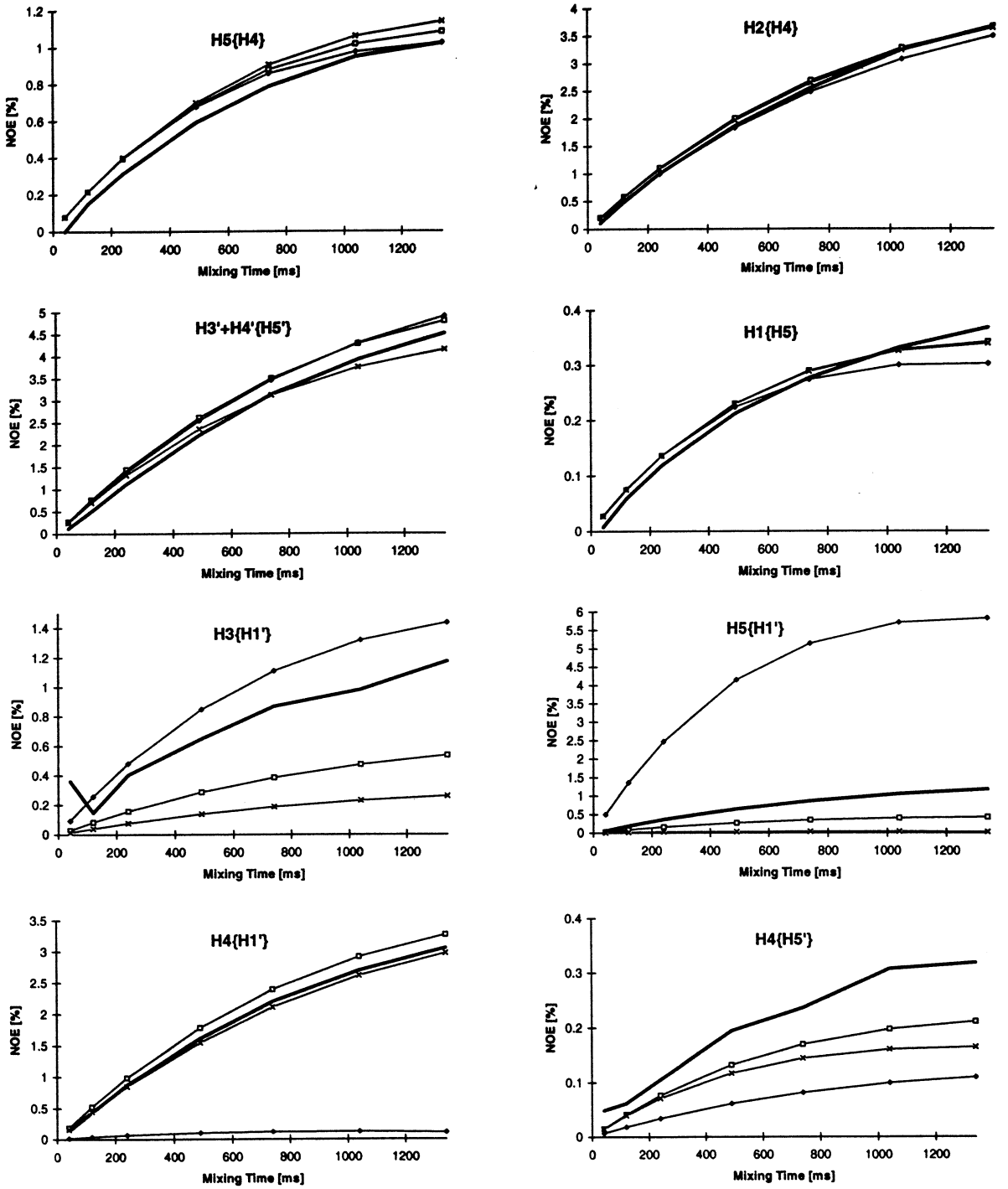

Fig. 8. Comparison of selected experimental and theoretical NOE curves for compound **2**. Experimental values are plotted with thick lines. Theoretical NOE curves represent (1) a Boltzmann averaging of grid search data neglecting all *tg*-conformations (—□—), (2) the global minimum-energy conformation **A** (Φ/Ψ $-49°/-18°$) (— × —), and (3) the local minimum-energy conformation **C** (Φ/Ψ $-50°/180°$) (—◆—).

favoured over the *gauche*, *anti* conformation **5**, and in equatorially oriented compounds, *anti*, *gauche* **6** is favoured over the *anti*, *anti* conformation **7** (Fig. 10) [19]. The conformational preferences and associated geometrical variations have been rationalised in terms of stabilising orbital interactions between the p-type nonbonding orbitals on X and Y, n_x and n_y, with the acceptor orbitals σ^*_{C-Y} and σ^*_{C-X}, respectively [19]. These hyperconjugative in-

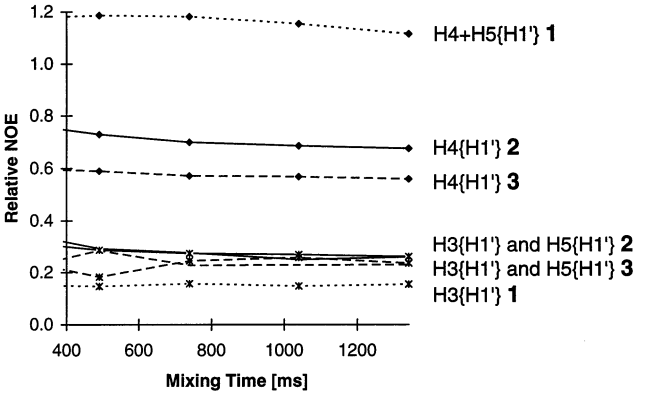

Fig. 9. Comparison of the relative magnitudes of interglycosidic NOE effects in compounds **1**–**3**. Experiments with short mixing times are not included due to a higher uncertainty of the data.

teractions account for the existence of the endo- and exo-anomeric effect when the $RXCH_2YR'$ moiety is incorporated into a heterocyclohexane (Fig. 10) [19]. The *gauche*, *gauche* conformation **4** is the global minimum when X and Y are first- or second-row elements. However, the stabilisation of the *gauche*, *anti* conformation **5** becomes as significant or more significant with elements of the third and fourth row owing to the importance of other stabilising orbital interactions [20]. The trend suggests that the population of this alternative conformation in **2** and **3** might still provide anomeric stabilisation. It is noteworthy that both conformational families for **1**–**3** in which the Φ angle is $-$*gauche* or $+$*gauche*, corresponding to **4** and **5**, respectively, are significantly populated.

3. Conclusions

NOE data in conjunction with Boltzmann-averaged grid search calculations give a good representation of the conformational features of the maltoside heteroanalogues investigated here. In general, the conformational families that are populated in these compounds are equivalent to those found for maltose. Substitution of oxygen in the interglycosidic linkage by sulfur or selenium results in an increase in flexibility. Increased flexibility, relative to the oxygen congeners, has also recently been reported for a cellobiose analogue [21a] and an α-Fuc-(1→3)-GlcNAc analogue [21b] containing sulfur atoms in the interglycosidic linkages.

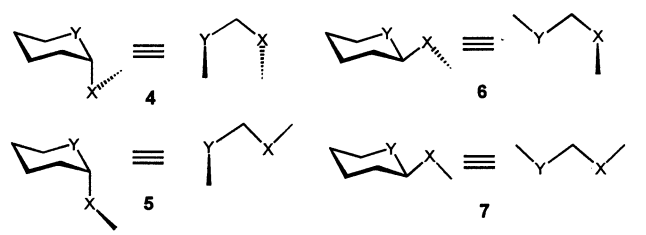

Fig. 10. Conformations of $RX–CH_2–YR'$ molecules and their relationships to the conformations of 2-substituted heterocyclohexanes.

The experimental NOEs for compounds **1** and **2** reveal some shortcomings of the molecular mechanics program (PIMM91) in that the C-5–C-6 rotamer distribution is not correctly predicted and that conformations in the global minimum-energy region are over-represented in the averaged structure used for the calculation of theoretical NOE data.

4. Experimental

NMR experiments.—Samples were prepared by repeatedly dissolving and lyophilising 10 mg of compounds **1**–**3** in D_2O. A final sample concentration of ca. 50 mM (0.5 mL D_2O (99.9%, ISOTEC Inc.)) was achieved. Several freeze–pump–thaw cycles were used to remove oxygen before the samples were sealed under nitrogen. NMR spectra were recorded on a Bruker AMX 600 spectrometer. NOE experiments were performed at 319 K for **2** and 316 K for **1** and **3**. Data acquisition and data treatment were performed as described previously [6,22]. In brief, 80 ms Gaussian-shaped, selective 180° pulses were used to invert the resonances of interest and were followed by the mixing time of the NOE experiment (41, 120, 240, 490, 740, 1040 and 1340 ms, corrected to incorporate NOE build up during the inversion pulse [23]). The enhancement was read by a 90° pulse at the end of the experiment. For each NOE spectrum, 256 experiments were added and on- and off-resonance data were subtracted during the phase cycle. A total of 8000 raw data were zero-filled to 16,000 prior to Fourier transformation. Data processing was achieved with

UXNMR (Bruker). NOE enhancements greater than 1% have an error of less than 5%, those between 0.5 and 1% have errors of 5–10%, and enhancements of less than 0.5% have errors up to 20%. Integration of NOEs from overlapping peaks was achieved with line deconvolution routines from UXNMR.

Computations.—All calculations were performed on SGI Personal Iris 4D/35 and SGI 380 Power series computers. The molecular mechanics program PIMM91 [3] was used. The hydrogen bond search routine was disabled for all computations to eliminate artificial stabilisations due to hydrogen bonding that would not be observed in an aqueous environment. First, a grid search was performed by permuting both of the ω angles and all of the hydroxyl group torsion angles to 60, 180 and 300° to give 2187 fully optimised structures. Contour searches were performed in which the interglycosidic torsion angles Φ and Ψ, i.e., H-1′–C-1′–X-4′–C-4 and C-1′–X-1′–C-4–H-4 (X = O or S), were permuted starting from 0° as well as from 360°, with an increment or decrease of 10°. These two angles were fixed at a particular value while the rest of the molecule was allowed to relax fully. For each of the nine possible conformations of the two ω angles, i.e., S-5–C-5–C-6–O-6, the contour search was performed independently. The starting orientation of the hydroxyl groups was chosen according to the predominant conformation, i.e., highest percentage distribution according to a Boltzmann averaging. Thus, 21,393 structures were calculated, and for each Φ/Ψ combination, the one lowest in energy was selected for the contour plot, independent of the corresponding orientation of the hydroxymethyl group. To calculate theoretical NOE data, *tg*-orientations of the hydroxymethyl group were neglected, and for the remaining conformations, the theoretical population was determined according to a Boltzmann averaging and those structures that exceeded 0.01% were selected. This resulted in 10,952 structures that were used to calculate averaged theoretical proton–proton distances on the basis of $\langle r^{-6} \rangle$, with weighting of each conformer according to its percentage contribution. The program CROSREL [24], which employs a full-relaxation matrix approach [25], was used to calculate theoretical NOE values, assuming isotropic motion and neglecting effects of strong scalar coupling [26] and cross-correlation [27], with an overall correlation time τ_c of 80 ps and a leakage rate of 0.05 Hz [28].

Acknowledgements

The authors are grateful to the Natural Sciences and Engineering Research Council of Canada for financial support. T.W thanks the Deutsche Forschungsgemeinschaft for a fellowship (WE 1818/2-1) and the Fonds der Chemischen Industrie.

References

[1] (a) E. Truscheit, W. Frommer, B. Junge, L. Müller, D.D. Schmidt, W. Wingender, *Angew. Chem., Int. Ed. Engl.*, 20 (1981) 744–761. (b) S. Omoto, J. Itoh, H. Ogino, K. Jwamatsu, N. Nishizawa, S. Inouye, *J. Antibiot.*, 34 (1981) 1429–1433. (c) B. Junge, F.-R. Heiker, K. Kurz, L. Müller, D.D. Schmidt, C. Wunsche, *Carbohydr. Res.*, 128 (1984) 235–268. (d) K. Bock, M. Meldal, S. Refn, *Carbohydr. Res.*, 221 (1991) 1–16. (e) H. Driguez, Thiooligosaccharides in glycobiology, in H. Driguez, J. Thiem (Eds.), *Topics in Current Chemistry*, Vol. 187, Springer, Berlin, 1997, pp. 85–116. (f) T. Suami, S. Ogawa, *Adv. Carbohydr. Chem. Biochem.*, 48 (1990) 21–90. (g) J.S. Andrews, B.M. Pinto, *Carbohydr. Res.*, 270 (1995) 51–62. (h) S. Mehta, K.L. Jordan, T. Weimar, U.C. Kreis, R.J. Batchelor, F.W.B. Einstein, B.M. Pinto, *Tetrahedron: Asymmetry*, 5 (1994) 2367–2396. (i) C.-H. Wong, T. Kracht, C. Gautheron-Le Navor, Y. Ichikawa, G.C. Look, F. Gaeta, D. Thompson, K.C. Nicolaou, *Tetrahedron Lett.*, 32 (1991) 4867–4870. (j) H. Yuasa, O. Hindsgaul, M.M.J. Palcic, *J. Am. Chem. Soc.*, 114 (1992) 5891–5892. (k) H. Hashimoto, M. Izumi, *Tetrahedron Lett.*, 34 (1993) 4949–4952. (l) K. Suzuki, H. Hashimoto, *Tetrahedron Lett.*, 35 (1994) 4119–4122. (m) H. Hashimoto, T. Fujimori, H. Yuasa, *J. Carbohydr. Chem.*, 9 (1990) 683–694. (n) H. Hashimoto, K. Shimada, S. Horito, *Tetrahedron: Asymmetry*, 5 (1994) 2351–2366. (o) H. Hashimoto, M. Kawanishi, H. Yuasa, *Carbohydr. Res.*, 282 (1996) 207–221. (p) H. Hashimoto, M. Kawanishi, H. Yuasa, *Chem. Eur. J.*, 2 (1996) 556–560. (q) M. Izumi, O. Tsuruta, S. Harayama, H. Hashimoto, *J. Org. Chem.*, 62 (1997) 992–998. (r) J.S. Andrews, T. Weimar, T.P. Frandsen, B. Svensson, B.M. Pinto, *J. Am. Chem. Soc.*, 117 (1995) 10799–10804. (s) J.S. Andrews, B.D. Johnston, B.M. Pinto, *Carbohydr. Res.*, 310 (1998) 27–33. (t) B.D. Johnston, B.M. Pinto, *Carbohydr. Res.*, 310 (1998) 17–25. (u) B.D. Johnston, B.M. Pinto, *J. Org. Chem.*, 63 (1998) 5797–5800. (v) M. Izumi, Y. Suhara, Y. Ichikawa, *J. Org. Chem.*, 63 (1998) 4811–4816.

[2] S. Mehta, J.S. Andrews, B.D. Johnston, B. Svensson, B.M. Pinto, *J. Am. Chem. Soc.*, 117 (1995) 9783–9790.

[3] (a) M. Kroeker, H.J. Lindner, Pi SCF Molecular Mechanics PIMM91, University of Darmstadt, 1991. (b) A.E. Smith, H.J. Lindner, *J. Comput. Aided Mol. Des.*, 5 (1991) 235–262.
[4] D. Neuhauss, M. Williamson, *The Nuclear Overhauser Effect in Structural and Conformational Analysis*, VCH Publishers, New York, 1989.
[5] A.S. Sashkov, G.M. Lipkind, N.K. Kochetkov, *Carbohydr. Res.*, 147 (1986) 175–182.
[6] T. Weimar, B. Meyer, T. Peters, *J. Biomol. NMR*, 3 (1993) 399–414.
[7] J.A. Gerlt, A.V. Youngblood, *J. Am. Chem. Soc.*, 102 (1980) 7433–7438.
[8] D.G. Streefkerk, M.J.A de Bries, J.F.G Vliegenthart, *Tetrahedron*, 29 (1973) 833–844.
[9] C.A.G. Haasnoot, F.A.A.M. de Leeuw, C. Altona, *Tetrahedron*, 36 (1980) 2783–2792.
[10] (a) M.J. Kroon-Batenburg, J. Kroon, *Biopolymers*, 29 (1990) 1243–1248. (b) R.K. Schmidt, B. Teo, J.W. Brady, *J. Phys. Chem.*, 99 (1995) 11339–11343.
[11] (a) K.-H. Ott, B. Meyer, *Carbohydr. Res.*, 281 (1996) 11–34. (b) J.W. Brady, R.K. Schmidt, *J. Phys. Chem.*, 97 (1993) 958–966.
[12] (a) R.J. Woods, R.A. Dwek, C.J. Edge, B. Fraser-Reid, *J. Phys. Chem.*, 99 (1995) 3832–3846. (b) R. Stuike-Prill, B. Meyer, *Eur. J. Biochem.*, 194 (1991) 903–919.
[13] (a) J.L. Asensio, J. Jiménez-Barbero, *Biopolymers* 35 (1995) 55–73. (b) J.L. Asensio, M. Martin-Pastor, J. Jiménez–Barbero, *Int. J. Biol. Macromol.*, 17 (1995) 137–148.
[14] R.J. Batchelor, F.W.B. Einstein, Unpublished data.
[15] P.J. Kraulis, *J. Appl. Crystallogr.*, 24 (1991) 946–950.
[16] B.M. Pinto, H.B. Schlegel, S. Wolfe, *Can. J. Chem.*, 65 (1987) 1658–1662.
[17] R.U. Lemieux, S. Koto, *Tetrahedron*, 30 (1974) 1933–1944.
[18] K. Bock, J.O. Duus, S. Refn, *Carbohydr. Res.*, 253 (1994) 51–67.
[19] B.M. Pinto, R.Y.N. Leung, The anomeric effect and associated stereoelectronic effects, in G.R.J. Thatcher (Ed.), *ACS Symposium Series*, Vol. 539, American Chemical Society, Washington, DC, 1993, Chapter 8, pp. 126–155.
[20] (a) S.L. Kahn, R.Y.N. Leung, J. Korppi-Tommola, B.M. Pinto, *J. Mol. Struct. Theochem.*, 303 (1994) 163–176. (b) U. Salzner, P.v.R. Schleyer, *J. Am. Chem. Soc.*, 115 (1993) 10231–10236.
[21] (a) E. Montero, M. Vallmitjana, J.A. Pérez-Pons, E. Querol, J. Jiménez-Barbero, F.J. Cañada, *FEBS Lett.*, 421 (1998) 243–248. (b) B. Aguielera, J. Jiménez-Barbero, A. Fernandéz-Mayoralas, *Carbohydr. Res.* 308 (1998) 19–27.
[22] T. Peters, T. Weimar, *J. Biomol. NMR*, 4 (1994) 97–116.
[23] P.J. Hajduk, D.A. Horita, L.E. Lerner, *J. Magn. Reson. A*, 103 (1993) 40–52.
[24] B.R. Leeflang, L.M.J. Kroon-Batenburg, *J. Biomol. NMR*, 2 (1992) 495–518.
[25] (a) R. Boelens, T.M.G. Koning, G.A. Van der Marel, J.H. Van Boom, R.J. Kaptein, *J. Magn. Reson.*, 82 (1989) 290–308. (b) B.A. Borgias and T.L. James, *Methods Enzymol.*, 176 (1989) 169–183.
[26] L.E. Kay, J.N. Scarsdale, D.R. Hare, J.H. Prestegard, *J. Magn. Reson.*, 68 (1986) 515–525.
[27] (a) T.E. Bull, *J. Magn. Reson.*, 72 (1987) 397–413. (b) V.V. Krishnan, A. Kumar, *J. Magn. Reson.*, 92 (1991) 293–311.
[28] K. Bock, H. Lönn, T. Peters, *Carbohydr. Res.*, 198 (1990) 375–380.